Elastic-viscoplastic notch correction methods

M. Chouman, Anais Gaubert, Jean Louis Chaboche, Pascale Kanoute, Georges Cailletaud, Stéphane Quilici

International Journal of Solids and Structures 51 (2014) 3025–3041

Contents lists available at ScienceDirect

International Journal of Solids and Structures

journal homepage: www.elsevier.com/locate/ijsolstr

Elastic-viscoplastic notch correction methods

M. Chouman [a,1], A. Gaubert [a,*,2], J.L. Chaboche [a,3], P. Kanouté [a], G. Cailletaud [b], S. Quilici [b]

[a] Dept. of Metallic Materials and Structures, ONERA, 29, Avenue de la Division Leclerc, 92322 Chatillon Cedex, France
[b] MINES ParisTech, Centre des matériaux, CNRS UMR 7633, BP 87, 91003 Evry Cedex, France

ARTICLE INFO

Article history:
Received 18 December 2013
Received in revised form 13 April 2014
Available online 4 May 2014

Keywords:
Neuber's type methods
Stress concentrations
Viscoplasticity

ABSTRACT

Neuber's type methods are dedicated to obtain fast estimation of elastic–plastic state at stress concentrations from elastic results. To deal with complex loadings, empirical rules are necessary and do not always give satisfying results. In this context, we propose a new approach based on homogenization techniques. The plastic zone is viewed as an inclusion in an infinite elastic matrix which results in relationships between the elastic solution of the problem and estimated stress–strain state at the notch tip. Three versions of the notch correction method are successively introduced, a linear one which directly uses Eshelby's solution to compute stresses and strains at the notch, a non-linear method that takes into account plastic accommodation through a β-rule correction and, finally, the extended method that is based on the transformation field analysis methods. All the notch correction methods need calibration of localization tensors. The corresponding procedures are proposed and analyzed. The methods are compared on different simulation cases of notched specimens and the predictive capabilities of the extended method in situations where plasticity is not confined at the notch are demonstrated. Finally, the case of a complex multiperforated specimen is addressed.

1. Introduction

Lifetime of structural components is often controlled by notches and stress concentrations where plasticity can develop. Finite element (FE) elastic–plastic or elastic-viscoplastic simulations of complex components can still be prohibitive in a design process. Consequently, there is a need for fast estimation methods of plasticity at stress concentrations.

Rules applying a plastic correction to deduce elastic–plastic stress and strain state from an elastic solution were developed to do so. Neuber (1961) was the first to propose such a method for uniaxial monotonic loading conditions. In case of notched bodies in plane stress, which results in a uniaxial stress state, he postulates a kind of local energetic equivalence between an elastic and an elastic–plastic calculation:

$$\sigma^e_{22}\epsilon^e_{22} = \sigma^p_{22}\epsilon^p_{22} \tag{1}$$

Later, Molski and Glinka (1981) developed a similar method assuming localized plasticity at the notch tip. In that case, the strain energy density at the notch tip can be approximated by that obtained if the body were to remain elastic:

$$\int_0^{\varepsilon^a} \sigma^p_{22} d\varepsilon^p_{22} = \frac{1}{2}\sigma^e_{22}\varepsilon^e_{22} \tag{2}$$

Theoretical justifications of those approaches have been proposed in the literature (Desmorat, 2002; Ye et al., 2004; Guo et al., 1998). They were also extended and improved over the last four decades. For example, Chaudonneret and Culié (1985) have worked on cyclic extensions.

One of the main issues with those methods arises when dealing with multiaxial stress states. In the general case of triaxial mechanical state at the notch root, three stress components, four strain components and four plastic strain components have to be computed locally. Elastic and plastic behavior laws provide 4 + 4 scalar equations. Consequently, three more equations are needed to solve the problem.

In the one hand, the approach followed in Hoffman and Seeger (1985) consists in generalizing the uniaxial Neuber rule using equivalent stress and strain quantities instead of uniaxial values. They add two more assumptions on (i) principal directions and (ii) ratios between the two first principal stresses to close the problem. In a similar way, Moftakhar et al. (1994) proposed multiaxial generalizations of Neuber's and Molski–Glinka's rules and assumes equality of the contribution of each stress–strain component in the

* Corresponding author. Tel.: +33 146734664.
E-mail addresses: anais.gaubert@snecma.fr (A. Gaubert), jean-louis.chaboche@onera.fr (J.L. Chaboche).
[1] Former research fellow at Onera.
[2] Former research scientist at Onera, now at Snecma, Groupe Safran.
[3] Principal corresponding author.

http://dx.doi.org/10.1016/j.ijsolstr.2014.04.017
0020-7683/

strain energy density between elastic and elastic–plastic computations.

On the other hand, researchers have worked on notch correction rules for non-proportional multiaxial loadings. Barkey et al. (1994) and Köttgen et al. (1995) incorporate directly the notch influence into the constitutive equation. An anisotropic structural yield surface in nominal stress space is then introduced. Another way to treat non-proportional loading sequences consists in applying the incremental formulation of generalized Neuber's rule as in Buczynski et al. (2003).

However, all the above presented methods suffer some limitations: (i) they are often limited to given geometries and (ii) they cannot take plastic redistributions into account. More recently Herbland et al. (submitted for publication) has proposed a completely new approach based on the Eshelby inclusion theory. The notch tip is viewed as an inclusion in an infinite matrix. The general formulation of this method allows the possibility to address non-proportional loading sequences for any material model. Herbland have also proposed a non-linear extension to take plastic redistributions around notch tip into account. Indeed, large plastic zones at notch tips are still challenging issues and most of Neuber's type methods fail in predicting plastic accomodation and ratcheting phenomenon.

The first objective of the present contribution is thus to discuss the predicting capabilities of Herbland's methods in non-confined plastic zone cases. This article aims also at presenting a new robust correction method that extends Herbland's work. It follows the same idea but it is derived from the transformation field analysis (TFA) (Dvorak and Benveniste, 1992) approach developed in the homogenization literature.

This contribution is organized as follows. Section 2 of this paper briefly sums up Herbland's linear and non-linear correction methods. The tested geometries and material models are presented in Section 3. Section 4 is dedicated to the application of both linear and non-linear Herbland's methods. The new correction method we propose is presented together with its application in Section 5. Finally, both Herbland's and the new correction method have been validated on a multiperforated specimen as described in Section 6.

2. Linear and non-linear notch correction methods

In Herbland's method (Herbland et al., submitted for publication), the plastic zone at notch tip is seen as an inclusion in a semi-infinite matrix. In the case of an infinite elastic matrix, Eshelby's solution links the stress in the inclusion $\underset{\sim}{\boldsymbol{\sigma}}^I$ and in the matrix $\underset{\sim}{\boldsymbol{\sigma}}^M$:

$$\underset{\sim}{\boldsymbol{\sigma}}^I = \underset{\sim}{\boldsymbol{\sigma}}^M + \underset{\approx}{\boldsymbol{C}} : \left(\underset{\sim}{\boldsymbol{\varepsilon}}^{pM} - \underset{\sim}{\boldsymbol{\varepsilon}}^{pI} \right) \tag{3}$$

where the superscript M denotes matrix quantities and the superscript I denotes inclusion quantities. The fourth order tensor $\underset{\approx}{\boldsymbol{C}}$ depends on the elastic properties of the material and the geometry of the inclusion. This type of stress redistribution is the basis of Kröner's model for polycrystals. It is valid at the onset of plastic flow. If the problem is restricted to confined plasticity at the notch tip, the plastic deformation in the matrix $\underset{\sim}{\boldsymbol{\varepsilon}}^{pM}$ is supposed to be equal to zero so that Eq. (3) reduces to:

$$\underset{\sim}{\boldsymbol{\sigma}}^I = \underset{\sim}{\boldsymbol{\sigma}}^M - \underset{\approx}{\boldsymbol{C}} : \underset{\sim}{\boldsymbol{\varepsilon}}^{pI} \tag{4}$$

In the notch correction framework and following Neuber's type of approaches, the superscript M stands for the quantities at the notch tip coming from the elastic computation and the superscript I denotes the quantities in the elastic–plastic case. Nevertheless, other definitions for $\underset{\sim}{\boldsymbol{\sigma}}^M$ are discussed in Herbland et al. (submitted for publication) (nominal stress, average over a volume around the notch tip). This method will be denoted CL in the following. In fact, the analogy with the homogenization models is not fully verified, since, due to the introduction of the free surface, the stress state is not uniform in the plastic zone, and some stress components are null.

As classically shown in the homogenization framework (Berveiller and Zaoui, 1978), this linear correction leads to elastic accomodation. Herbland proposed an extension of his method to take into account plastic accomodation, still using tools from the homogenization literature. He applied the β-rule (Cailletaud, 1987) which consists in replacing the plastic strain $\underset{\sim}{\boldsymbol{\varepsilon}}^{pI}$ by an auxiliary variable $\underset{\sim}{\boldsymbol{\beta}}^I$ whose evolution is governed by a non-linear equation. More precisely, Herbland proposed the following evolution equation for $\underset{\sim}{\boldsymbol{\beta}}^I$ to control ratcheting effect:

$$\dot{\underset{\sim}{\boldsymbol{\beta}}}^I = \dot{\underset{\sim}{\boldsymbol{\varepsilon}}}^{pI} - \underset{\approx}{\boldsymbol{D}} : \left(\underset{\sim}{\boldsymbol{\beta}}^I - \underset{\approx}{\boldsymbol{\delta}} : \underset{\sim}{\boldsymbol{\varepsilon}}^{pI} \right) \| \dot{\underset{\sim}{\boldsymbol{\varepsilon}}}^{pI} \| \tag{5}$$

The tensor $\underset{\approx}{\boldsymbol{\delta}}$ is introduced to limit the ratcheting effect due to the non-linear term. It is diagonal and writes, using Voigt notations:

$$\underset{\approx}{\boldsymbol{\delta}} = \begin{pmatrix} \delta & 0 & 0 & 0 & 0 & 0 \\ 0 & \delta & 0 & 0 & 0 & 0 \\ 0 & 0 & \delta & 0 & 0 & 0 \\ 0 & 0 & 0 & \delta/2 & 0 & 0 \\ 0 & 0 & 0 & 0 & \delta/2 & 0 \\ 0 & 0 & 0 & 0 & 0 & \delta/2 \end{pmatrix} \tag{6}$$

Herbland's non-linear correction method will be denoted CNL in the following.

The linear and non-linear methods are summed up by Fig. 1. In a first step, the tensor $\underset{\approx}{\boldsymbol{C}}$ (plus $\underset{\approx}{\boldsymbol{D}}$, δ for the non-linear method) are calibrated through FE simulations. As it will be explained later, assumptions on the shape of those tensors can be made to reduce the number of parameters to be identified. First, an elastic-visco-plastic FE simulation on a monotonic or few cycles (typically 5 cycles) will be used as a reference. Then, an elastic simulation is performed to get $\underset{\sim}{\boldsymbol{\sigma}}^M$ at notch tip. This elastic simulation is post-processed to estimate the stress and strain fields at notch tip using Eq. (4) and the constitutive equations of the material. Reference values and notch correction values for $\underset{\sim}{\boldsymbol{\sigma}}$ and $\underset{\sim}{\boldsymbol{\varepsilon}}$ are then compared in an optimization loop to obtain the optimal values for the method parameters $\underset{\approx}{\boldsymbol{C}}$, $\underset{\approx}{\boldsymbol{D}}$, δ. In a second step, the notch correction method can be used on the same geometry and for the same

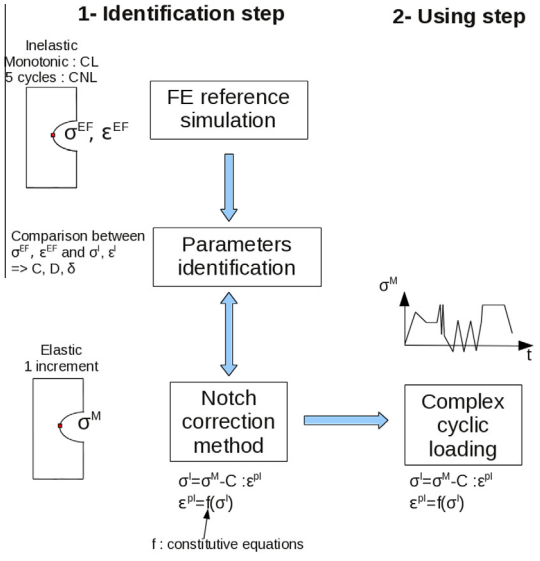

Fig. 1. Schematic view of the linear and non linear correction methods.

material to estimate the response at the critical point for any complex loading and over a large number of cycles instead of performing costly FE simulations of the whole problem.

In Herbland et al. (submitted for publication), the correction methods are applied under complex loadings such as variable amplitude or non-proportional tension–torsion loadings. A good agreement with FE simulations is reported. In particular, the non-linear method gives precise results in the case of non-confined plasticity at the notch. The present contribution is focused on the latter point. Two types of notched specimens and two types of materials are used to compare the predicting capabilities of the methods depending on plasticity confinement.

3. Test cases

This section presents the tested geometries and material models. Results with two different geometries and two different materials will be detailed in the present contribution to show the range of capabilities of the notch correction methods.

The two axisymmetric notched specimens with $k_t = 2$ and $k_t = 1.32$ that have been used differ in the sizes of plastic zone, the latter leading to non-confined plasticity. Fig. 2 presents the $k_t = 1.32$ and $k_t = 2$ meshes used to carry out the simulations. Both have approximatively 1900 axisymmetric quadratic reduced elements. Simulations are run using the Z-set FE software (Z-set). Axial mechanical loadings are applied.

The full finite element inelastic analyses are used for the complete calculations performed over thousands of cycles in order to capture the reference solutions. The same inelastic analyses, with the same meshes and constitutive parameters, are performed (over one monotonic loading or a few cycles), that serve to calibrate the parameters of the notch correction methods.

Two types of material models are tested. The first one represents a titanium alloy, TA6V at 200 °C and the second one is an isotropic (von Mises criterion) version of a model representing AM1 at high temperature (around 1000 °C). TA6V and AM1 exhibit very different behaviors. Consequently, they represent different kind of difficulties for notch correction methods. In a first hand, the TA6V mechanical behavior shows cyclic softening and non-zero mean stress values at stabilization for repeated fatigue loadings. For this material, the challenge consists therefore in being able to describe correctly those quantities together with deformations evolutions. In a second hand, the AM1 behavior is characterized by viscosity and creep which can generate plastic accomodation and large plastic zones at stress concentrations.

The corresponding material models are briefly described in the following sections.

3.1. Material 1: TA6V at 200 °C

TA6V is a titanium alloy widely used in the aeronautical industry. Its viscoplastic behavior at 200 °C is characterized by superposition of several hardening variables:

- one non-linear isotropic hardening;
- four non-linear kinematic hardening with threshold;
- one non-linear kinematic hardening (without threshold).

The constitutive model is described in Chaboche et al. (2012). Kinematic hardening with threshold are introduced to describe the non-fully mean stress relaxation during repeated fatigue tests. A high value of exponent in Norton's power law is considered to describe the low viscosity behavior of this material at 200 °C.

3.2. Material 2: AM1 at high temperature (around 1000 °C)

AM1 is a single crystal Ni-base superalloy designed for turbine blade applications in the aero-engine industry. This kind of materials works at temperatures up to 1150 °C. A double viscosity constitutive model is employed here, with an isotropic von Mises criterion. In this model, two viscoplastic potentials are defined. The first one carries the "fast" viscoplastic phenomena appearing during monotonic and cyclic tests. The second one is introduced to catch the "slow" viscoplastic effects appearing during creep or relaxation tests. The model falls into the two mechanisms and two criteria (2M2C) class of models (Chaboche, 2008). A non-linear kinematic hardening, together with a constant yield stress is associated to the first viscosity potential whereas no hardening variables nor yield stress appear in the second potential criterion. Norton's flow rules are adopted for both potentials. It should be noticed that, for the sake of simplicity, the isotropic version of the model is used here despite the anisotropic mechanical behavior of this kind of material.

4. Application of linear and non-linear correction methods

4.1. Implementation and identification procedure

Herbland's linear and non-linear methods have been implemented as a plug-in in the FE software Z-set. Critical point quantities $\underset{\sim}{\boldsymbol{\sigma}}^I$, $\underset{\sim}{\boldsymbol{\varepsilon}}^I$, $\underset{\sim}{\boldsymbol{\varepsilon}}^{pl}$ and all the internal variables of the considered material model are calculated at each time step using relations of Section 2. A second order Runge–Kutta scheme with automatic time stepping is used to compute evolution of internal variables.

The fourth order tensors in Eqs. (4) and (5) have to be calibrated on FE simulations. As said previously they depend on the material and geometry of the problem. In the case of an axisymmetric notched specimen in tension–compression, and using Voigt notations in cylindrical frame ($1 = r,\ 2 = z,\ 3 = \theta$), the stress and strain tensors at the notch tip (free surface) are reduced to the following expressions:

$$\underset{\sim}{\boldsymbol{\sigma}} = \begin{pmatrix} 0 \\ \sigma_2 \\ \sigma_3 \\ 0 \\ 0 \\ 0 \end{pmatrix} \qquad \boldsymbol{\varepsilon} = \begin{pmatrix} \varepsilon_1 \\ \varepsilon_2 \\ \varepsilon_3 \\ 0 \\ 0 \\ 0 \end{pmatrix} \tag{7}$$

To insure $\sigma_1 = 0$ at the notch tip, the fourth order tensors $\underset{\approx}{\boldsymbol{C}}$ and $\underset{\approx}{\boldsymbol{D}}$ can be reduced to:

$$\underset{\approx}{\boldsymbol{C}} = \begin{pmatrix} 0 & 0 & 0 & 0 & 0 & 0 \\ 0 & C_{22} & C_{23} & 0 & 0 & 0 \\ 0 & C_{23} & C_{33} & 0 & 0 & 0 \\ 0 & 0 & 0 & 0 & 0 & 0 \\ 0 & 0 & 0 & 0 & 0 & 0 \\ 0 & 0 & 0 & 0 & 0 & 0 \end{pmatrix} \tag{8}$$

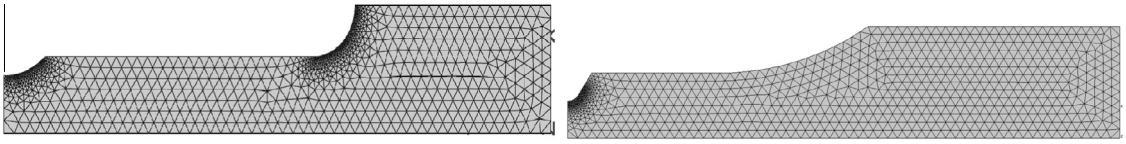

Fig. 2. $k_t = 1.32$ (top) and $k_t = 2$ (above) specimens meshes. The x_2 axis coincides with the axis of the specimens.

$$\underset{\approx}{\boldsymbol{D}} = \begin{pmatrix} 0 & 0 & 0 & 0 & 0 & 0 \\ 0 & D_{22} & D_{23} & 0 & 0 & 0 \\ 0 & D_{23} & D_{33} & 0 & 0 & 0 \\ 0 & 0 & 0 & 0 & 0 & 0 \\ 0 & 0 & 0 & 0 & 0 & 0 \\ 0 & 0 & 0 & 0 & 0 & 0 \end{pmatrix} \tag{9}$$

Consequently, only three values have to be calibrated in that case for the linear correction method (C_{22}, C_{33}, C_{23}) and seven for the non-linear method (C_{22}, C_{33}, C_{23}, D_{22}, D_{33}, D_{23}, δ).

The calibration procedure consists in searching parameters such as the correction method results match reference elastic-(visco) plastic FE results at the notch tip. To do so, optimization schemes such as the Levengberg–Marquart algorithm available in the Zsimopt environment of the Zset software (Z-set) is used into an automatic optimization loop. In the case of the linear correction method, a single monotonic loading is enough to identify the parameters. In the case of the non-linear correction method, Herbland recommands 1.5 cycle of a repeated fatigue test for the optimization procedure. In each case the full FE models of Fig. 2 are used, together with the proper constitutive equations of the materials.

4.2. Application of the linear correction method on the TA6V specimens

The first simulations have been run on the TA6V $K_t = 2$ specimen at 200 °C. This section presents the results of the linear correction method. The correction parameters are identified on the first 1/2 cycle (i.e. first monotonic tension) of a repeated fatigue test at 5 Hz under 605 MPa, computed by the full FE model.

The optimization procedure leads to the following parameters: $C_{22} = 7.70 \times 10^4$ MPa, $C_{33} = 1.55 \times 10^5$ MPa, $C_{23} = 2.40 \times 10^4$ MPa. Fig. 3(a) and (b) present the comparison between the full FE simulation result at the critical point and the results obtained using the notch correction method for 4000 simulated cycles. As it can be observed, the first monotonic loading which has been used for identification is very well described. The cyclic evolution of 22 and 33 stress components are correctly predicted, leading to a good agreement on the stress amplitude and mean stress values. Concerning the deformations, their estimated amplitude is consistent with the FE simulation but the mean value of ε_{22} is underestimated.

The method has been applied with the previously calibrated parameters on a second repeated fatigue test with $\sigma^{nom}_{max} = 454$ MPa (3(c) and (d)). They give a very good agreement in the axial direction as it can be observed in Fig. 3(c) and (d) whereas the mean value of ε_{33} is overestimated.

The choice of the loading condition used for the parameter calibration appears to be important. Indeed, notch correction method results are less good if the tensor $\boldsymbol{C}$ is identified on the $\sigma^{nom}_{max} = 454$ MPa loading as presented in Fig. 4. It shows that this second calibration leads to largely under-estimated mean values of ε_{22} et ε_{33} for both 454 MPa and 605 MPa tests. It can be concluded that the calibration of the notch correction method parameters should be made on the higher value in the range of the applied loadings that have to be simulated.

The work has also been done on the $K_t = 1.32$ geometry under repeated fatigue loading with $\sigma^{nom}_{max} = 852$ MPa. The identification procedure (over one monotonic loading) results in the following parameters: $C_{22} = 1.21 \times 10^5$ MPa, $C_{33} = 6.81 \times 10^5$ MPa, $C_{23} = 2.21 \times 10^5$ MPa. Results are plotted in Fig. 5. Here ratcheting of the deformation is largely under-estimated. Concerning stress fields, Their amplitudes after 4000 cycles given by the linear correction method and the FE results at notch tip are nearly the same. However, the cyclic mean value of σ_{33} is not correctly estimated by the method.

The non-confinement of plasticity for the specimen $K_t = 1.32$ explains the less good results obtained compared to the ones for $K_t = 2$. The accumulated plastic strain maps at the end of the first cycle in both cases are plotted in Fig. 6. It can be noticed that the plasticity develops in a large part of the $K_t = 1.32$ specimen whereas it is confined to the notch tip in the $K_t = 2$ geometry. Thus, it can be concluded that the linear correction method gives good results only when the plastic zone is small enough to ensure elastic shakedown all around the zone near the notch.

4.3. Application of the non-linear correction method on the TA6V specimens

Non-linear Herbland's correction method has also been tested. It has been exploited by performing first a full cyclic inelastic analysis with the FE models shown Fig. 2, over 5 successive cycles. From our experience, the optimization procedure is complex here because it appears that multiple sets of parameters can be found. Depending on their initial value, the optimization algorithm leads to very different sets of parameters, that probably means the existence of local minima. Fig. 7(a) and (b) show the results for an initial value of δ equal to 0 (leading to a final value $\delta = 0.51$) whereas Fig. 7(c) and (d) show the results for an initial value of δ equal to 1 (leading to a final value for $\delta = 1$).

As in the case of the linear correction method, evolution of σ_{22} and σ_{33} is correctly estimated so that their amplitudes and mean values at the stabilized cycle are in good agreement with the FE simulation. On the contrary, it is difficult to catch the right evolution for the deformation components. In particular, the first set of parameters, presented in Fig. 7(a) and (b), leads to much too large ratcheting effect. Concerning the second set, the accumulation of deformation is controlled by the high value of δ. The non-linear method is, in that case, close to the linear one that has given satisfactory results for the $K_t = 2$ geometry. Tests have been performed to identify parameters on five cycles instead of 1.5 cycle but it does not decrease the dependency of the parameters on their initial value nor increase the quality of the estimated results.

The interest of the non-linear method is pointed out for the $K_t = 1.32$ specimen. It gives much better results in that case than the linear one. Fig. 8 shows that the method predicts a large ratcheting during the first 200 cycles which stabilize after 1000 cycles. At the end of the 4000 simulated cycles, ε_{22} and ε_{33} are slightly over-estimated but this simulation clearly shows the capabilities of this method. The identified parameters are: $C_{22} = 2.0 \times 10^5$ MPa, $C_{33} = 7.10 \times 10^5$ MPa, $C_{23} = 2.73 \times 10^5$ MPa, $D_{22} = 6.71 \times 10^2$, $D_{33} = 1.94 \times 10^3$, $D_{23} = 7.06 \times 10^2$ and $\delta = 0.155$.

4.4. Application of the linear correction method on the AM1 specimens

The same kind of results are obtained with the AM1 material for the $K_t = 1.32$ geometry. Fig. 9 shows fatigue and creep simulation results with the linear correction method. As previously, C_{22}, C_{33} and C_{23} have been calibrated at 950 °C by the full FE analysis performed for the first tension of a 600 MPa repeated fatigue test at 5 Hz. Their values are: $C_{22} = 5.70 \times 10^4$ MPa, $C_{33} = 9.52 \times 10^4$ MPa, $C_{23} = 2.76 \times 10^4$ MPa. Comparisons with the reference FE simulations show that the method is not able to describe creep results or ratcheting results during repeated fatigue tests. It can also be noticed that the AM1 constitutive model leads, for each stress component, to a zero mean value at the stabilized cycle. Therefore, even if the strain evolutions are not correct, the stress amplitude and mean values predicted by the method are here consistent with the reference simulations.

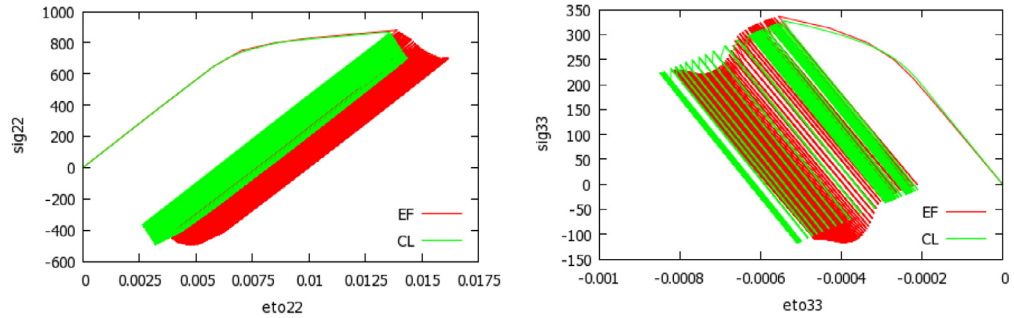

(a) σ_{max}^{nom}=605 MPa, axial components (b) σ_{max}^{nom}=605 MPa, hoop components

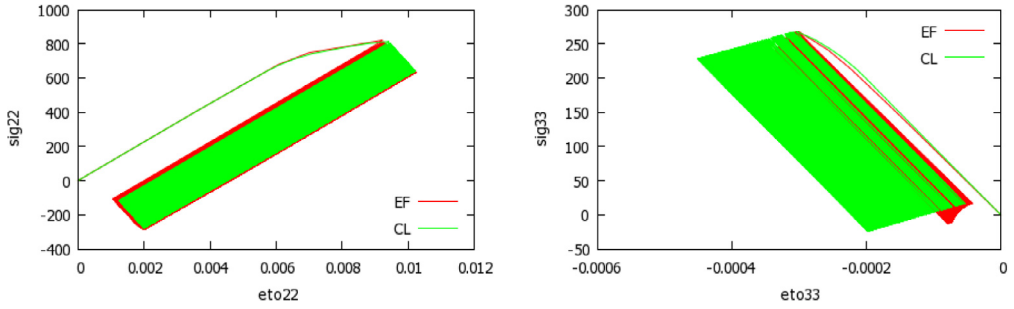

(c) σ_{max}^{nom}=454 MPa, axial components (d) σ_{max}^{nom}=454 MPa, hoop components

Fig. 3. Application of the linear correction method in the case of repeated 5 Hz fatigue simulations on TA6V K_t = 2 specimens. Calibration has been made on the first monotonic tension of the σ_{max}^{nom} = 605 MPa loading. Correction method results are plotted in green and compared to elastic-viscoplastic FE simulations in red. (For interpretation of the references to color in this figure legend, the reader is referred to the web version of this article.)

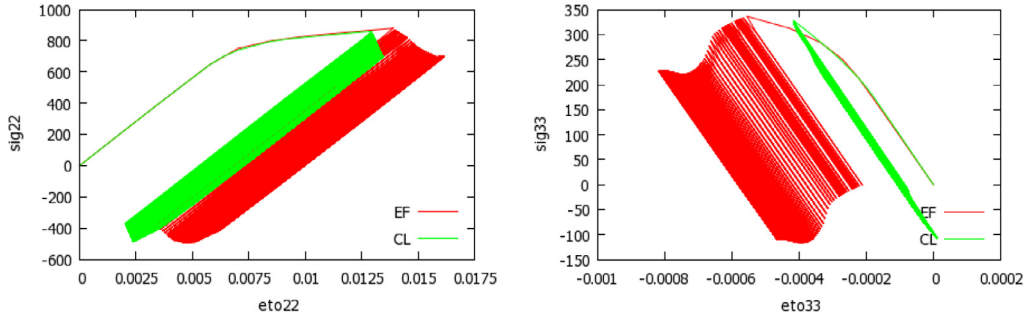

(a) σ_{max}^{nom}=605 MPa, axial components (b) σ_{max}^{nom}=605 MPa, hoop components

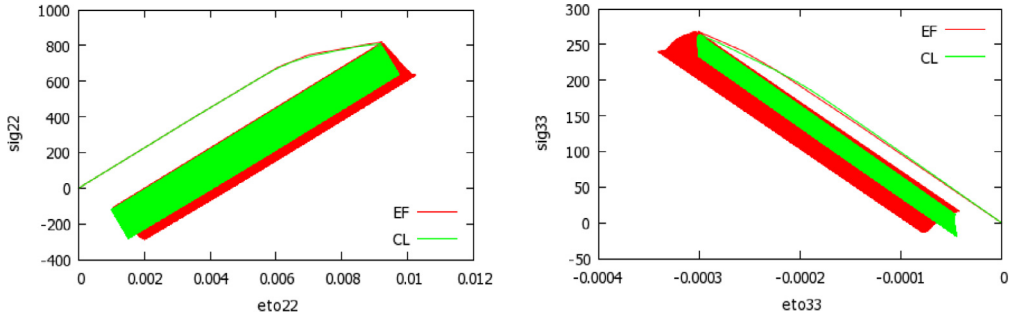

(c) σ_{max}^{nom}=454 MPa, axial componants (d) σ_{max}^{nom}=454 MPa, axial components

Fig. 4. Application of the linear correction method in the case of repeated 5 Hz fatigue simulations on TA6V K_t = 2 specimens. Compared to Fig. 3, calibration has been made on the first monotonic tension of the σ_{max}^{nom} = 454 MPa loading. Correction method results are plotted in green and compared to elastic-viscoplastic FE simulations in red. (For interpretation of the references to color in this figure legend, the reader is referred to the web version of this article.)

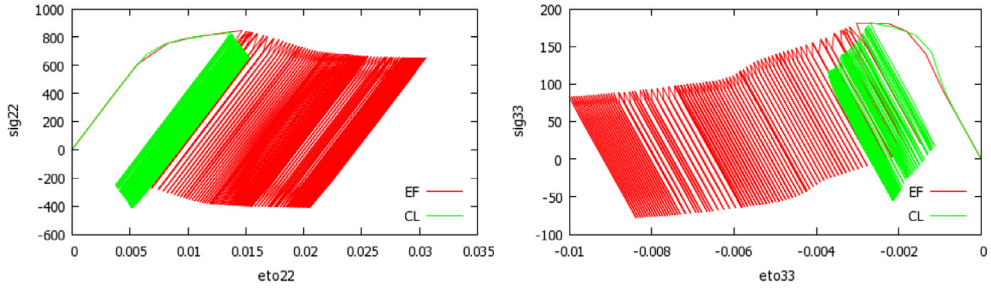

(a) σ_{max}^{nom}=852 MPa, axial components (b) σ_{max}^{nom}=852 MPa, hoop components

Fig. 5. Application of the linear correction method in the case of repeated 5 Hz fatigue simulations on TA6V K_t = 1.32 specimens.

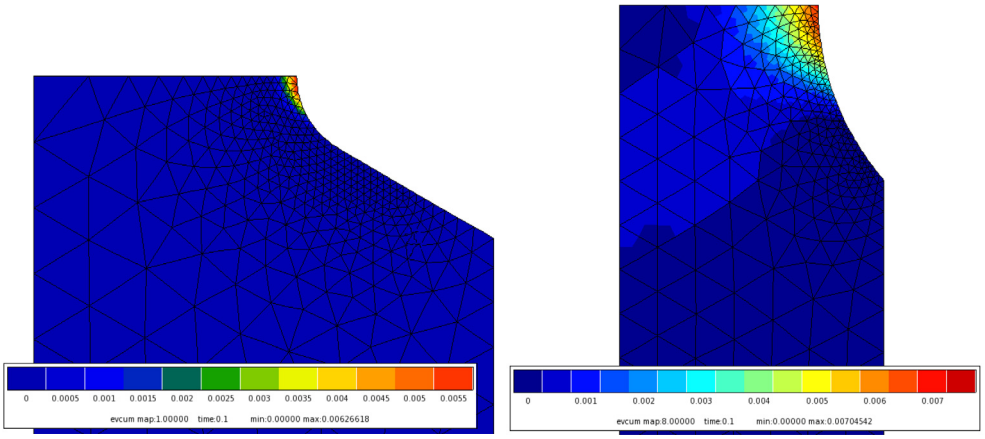

(a) K_t=2 (b) K_t=1.32

Fig. 6. Accumulated plastic strain fields at the end of the first cycle for both K_t = 2 and K_t = 1.32 specimens.

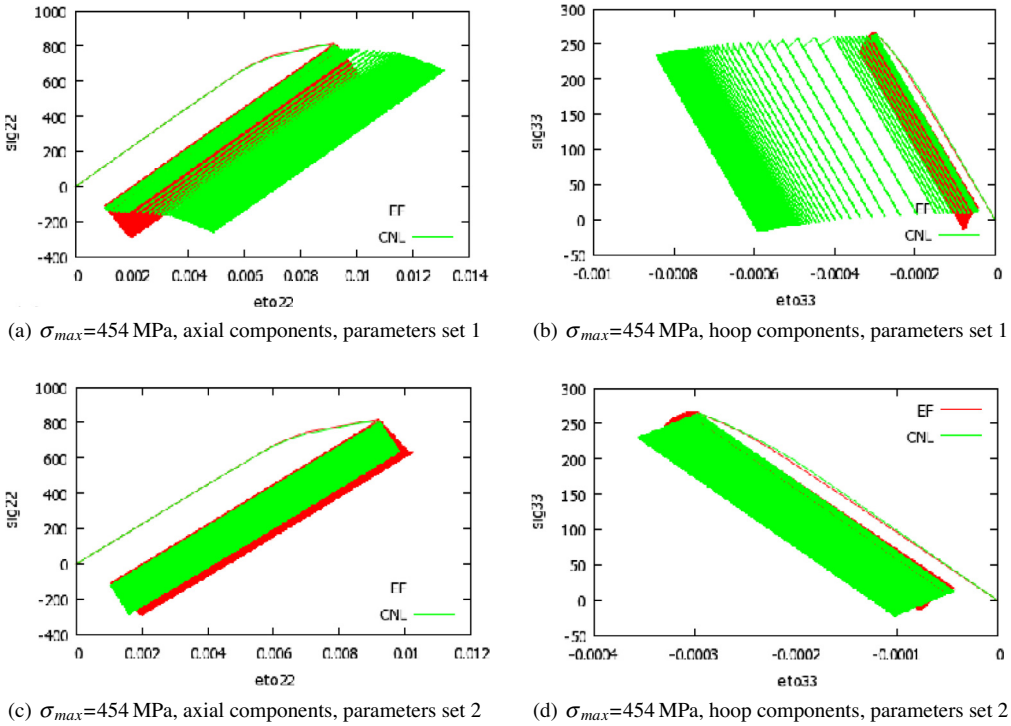

(a) σ_{max}=454 MPa, axial components, parameters set 1 (b) σ_{max}=454 MPa, hoop components, parameters set 1

(c) σ_{max}=454 MPa, axial components, parameters set 2 (d) σ_{max}=454 MPa, hoop components, parameters set 2

Fig. 7. Application of the non-linear correction method in the case of repeated 5 Hz fatigue simulations on TA6V K_t = 2 specimens. Two sets of parameters are presented to illustrate the difficulties in their identification due to non-uniqueness.

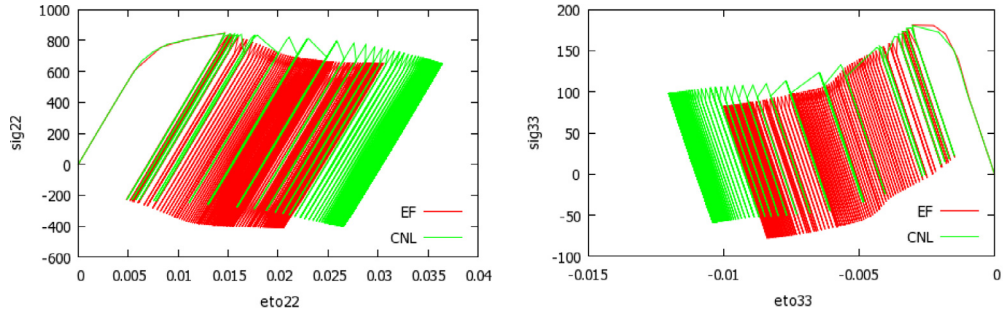

(a) σ_{max}^{nom}=850 MPa, axial components (b) σ_{max}^{nom}=850 MPa, hoop components

Fig. 8. Application of the non-linear correction method in the case of repeated 5 Hz fatigue simulations on TA6V K_t = 1.32 specimens. Correction method results are plotted in green and compared to elastic-viscoplastic FE simulations in red. (For interpretation of the references to color in this figure legend, the reader is referred to the web version of this article.)

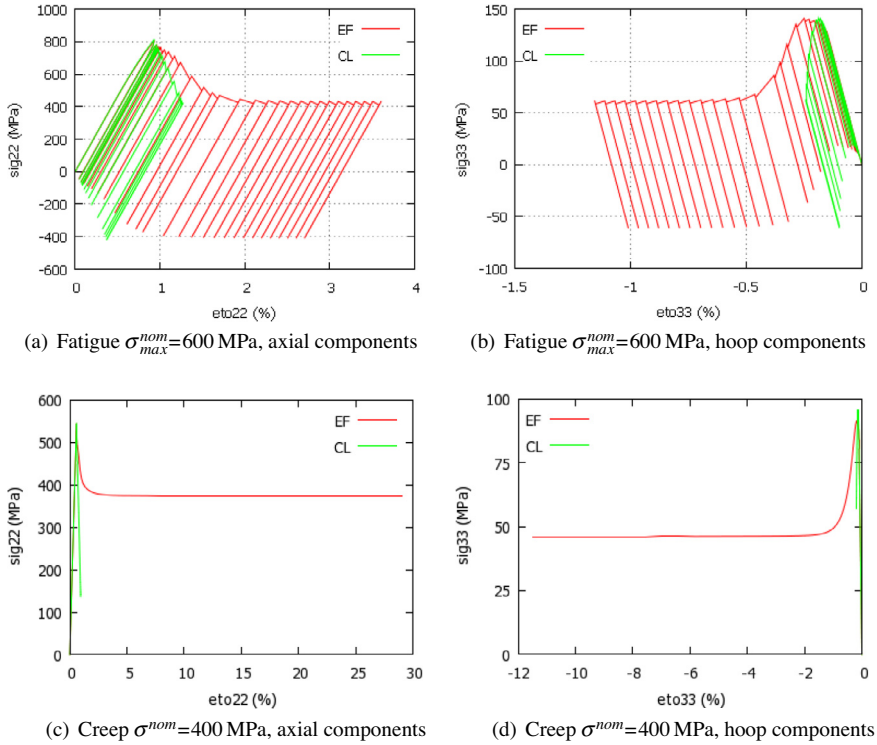

(a) Fatigue σ_{max}^{nom}=600 MPa, axial components (b) Fatigue σ_{max}^{nom}=600 MPa, hoop components

(c) Creep σ^{nom}=400 MPa, axial components (d) Creep σ^{nom}=400 MPa, hoop components

Fig. 9. Application of the linear correction method in the case of repeated 5 Hz fatigue and creep simulations on AM1 K_t = 1.32 specimens. Correction method results are plotted in green and compared to elastic-viscoplastic FE simulations in red. (For interpretation of the references to color in this figure legend, the reader is referred to the web version of this article.)

4.5. Application of the non-linear correction method on the AM1 specimens

Finally, the non-linear correction method has been applied to the K_t = 1.32 AM1 specimens. In that case, different calibration strategies have been tested depending on the chosen loading condition, fatigue or creep, and the number of cycles/time considered at the calibration stage. The parameters used to plot the results in Fig. 10 have been identified on a 400 MPa creep simulation at 950 °C. As it can be observed, those parameters lead to over-estimated ratcheting effect and over-estimated mean stresses reached at the stabilized cycle on the simulation of a repeated fatigue test in comparison to the full FE simulations. It is interesting to notice that the identified δ value is 0.0. The other parameters are: $C_{22} = 2.76 \times 10^4$ MPa, $C_{33} = 1.39 \times 10^5 \times$ MPa, $C_{23} = 2.23 \times 10^4$ MPa, $D_{22} = 6.40 \times 10^1$, $D_{33} = 1.28 \times 10^2$, D_{23} = 0.0.

4.6. Conclusions on the linear and non-linear methods

To conclude this analysis of Herbland's correction methods, we can say that they are promising tools to get a fast estimation of stress and strain states at the notch tip. The linear correction method gives good results when plasticity is confined at notch tip. Moreover calibration of the parameters in that case is quite easy. However, it fails to estimate ratcheting effect or creep deformation when the plastic zone is too large. In the other hand, the non-linear correction can take plastic accomodation into account but convergence of the optimization algorithm and the existence

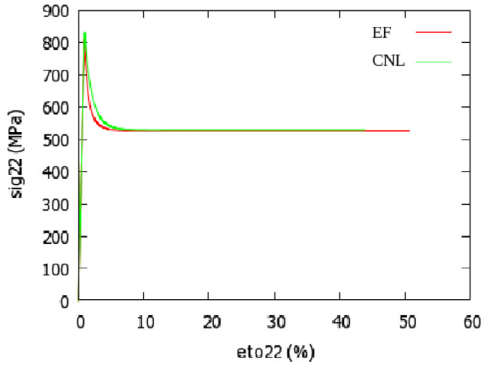

(a) Creep under 400 MPa, axial components

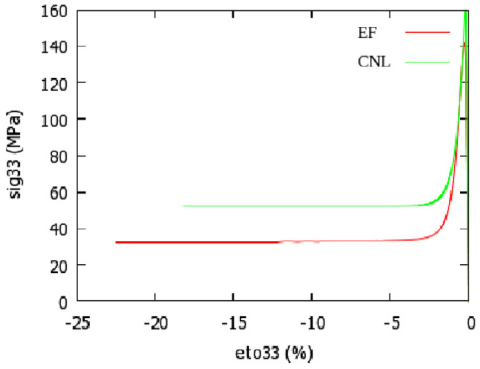

(b) Creep under 400 MPa, hoop components

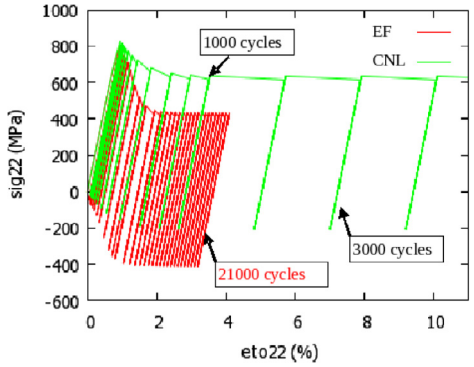

(c) Fatigue σ_{max}=600 MPa, axial components

Fig. 10. Application of the non-linear correction method in the case of 400 MPa creep and repeated 5 Hz fatigue simulations on AM1 K_t = 1.32 specimens. Correction parameters are identified on the creep simulation.

of multiple solutions make the calibration procedure more complex.

5. New correction method

In order to circumvent the drawbacks of non-linear Herbland's correction method, we propose a new method that will be called the new correction method and abbreviate MC in the following.

5.1. Background

In order to take plastic accomodation into account, the plastic zone is still viewed as an inclusion in an elastic matrix but with different elastic properties between the matrix and the inclusion. The stress in the inclusion is linked to the macroscopic one by a localization rule that writes:

$$\underset{\sim}{\boldsymbol{\sigma}}^{I} = \underset{\approx}{\boldsymbol{B}} : \underset{\sim}{\boldsymbol{\Sigma}} + \underset{\approx}{\boldsymbol{C}} : \left(\underset{\sim}{\boldsymbol{E}}^{p} - \underset{\sim}{\boldsymbol{\varepsilon}}^{pl} \right) \tag{10}$$

where $\underset{\sim}{\boldsymbol{\Sigma}}$ and $\underset{\sim}{\boldsymbol{E}}^{p}$ represent macroscopic stress and plastic strain tensors. $\underset{\approx}{\boldsymbol{B}}$ is a fourth order stress concentration tensor and plays the role of a stress concentration factor K_t in the proposed approach. $\underset{\approx}{\boldsymbol{C}}$ is a fourth order influence tensor. Eq. (10) can be deduced from the TFA approach for phases with inhomogeneous elastic properties (Dvorak and Benveniste, 1992).

The macroscopic stress $\underset{\sim}{\boldsymbol{\Sigma}}$ plays the role of a nominal stress and is defined as the average of stresses from an elastic simulation over a sphere around the notch tip, whose diameter R is a geometrical parameter to identify:

$$\Sigma_{ij} = \frac{1}{V(R)} \int_{V(R)} \sigma_{ij} dV \tag{11}$$

$\underset{\sim}{\boldsymbol{E}}^{p}$ is introduced to account for non confined plasticity in the specimen. It is calculated from the nominal elastic stress $\underset{\sim}{\boldsymbol{\Sigma}}$ using the constitutive equations of the material. Consequently, the proposed method is characterized by three quantities to be calibrated: $\underset{\approx}{\boldsymbol{B}}$, $\underset{\approx}{\boldsymbol{C}}$ and R. Finally, both Herbland's methods and the new correction one require the same input: the response of the structure over one elastic increment. The difference between them arises in the definition of the input stress. Herbland's method directly uses the elastic stress at the critical point whereas the nominal stress in the new method is defined by its average value over a small volume around the notch tip. Moreover, in the latter method, two internal variables $\underset{\sim}{\boldsymbol{E}}^{p}$ and $\underset{\sim}{\boldsymbol{\varepsilon}}^{pl}$ have to be integrated all along the applied loading instead of one in the case of Herbland's methods. Accordingly, $\underset{\sim}{\boldsymbol{\sigma}}^{M}$ and $\underset{\sim}{\boldsymbol{\Sigma}}$ along the applied loading are deduced from the elastic FE simulation using the linear features of this kind of simulation.

When dealing with confined plasticity, the plastic strain tensor associated with $\underset{\sim}{\boldsymbol{\Sigma}}$ is negligible and Eq. (10) reduces to:

$$\underset{\sim}{\boldsymbol{\sigma}}^{I} = \underset{\approx}{\boldsymbol{B}} : \underset{\sim}{\boldsymbol{\Sigma}} - \underset{\approx}{\boldsymbol{C}} : \underset{\sim}{\boldsymbol{\varepsilon}}^{pl} \tag{12}$$

The product $\underset{\approx}{\boldsymbol{B}} : \underset{\sim}{\boldsymbol{\Sigma}}$ is equal to the local elastic stress at the critical point used in Herbland's method and denoted $\underset{\sim}{\boldsymbol{\sigma}}^{M}$. Therefore, Eq. (10) reduces to Eq. (4) in case of confined plasticity. In other words, the new method proposed here is an extension of the linear method from Herbland.

Fig. 11 illustrates both methods in the particular case of a monotonic loading. In Herbland's method, the elastic stress at the notch tip is directly taken from the FE simulation. Elastic-viscoplastic stress and strain fields at the critical point are deduced from Eq. (4). In the schematic monotonic and uniaxial view of Fig. 11, this equation consists in using a linear relationship, whose

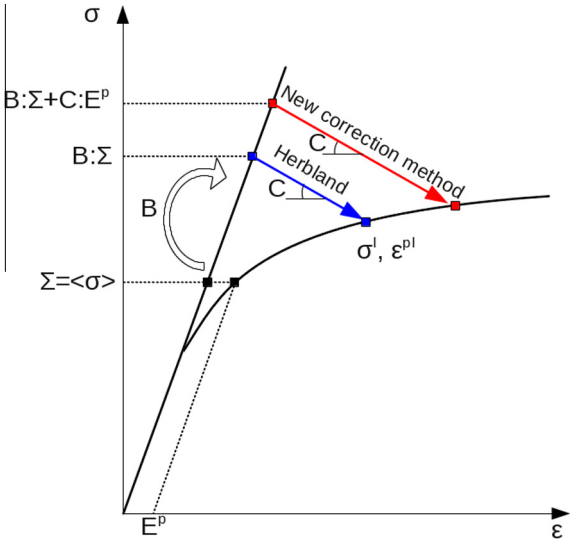

Fig. 11. Schematic view of Herbland's linear correction method and the new correction method.

slope is defined by the tensor $\underset{\approx}{\boldsymbol{C}}$, to deduce $\underset{\sim}{\boldsymbol{\sigma}}^{I}$ and $\underset{\sim}{\boldsymbol{\varepsilon}}^{pI}$. In the new correction method, the input is the average elastic stress field around the notch tip. The nominal plastic strain field is characterized by $\underset{\sim}{\boldsymbol{E}}^{p}$ which is computed from the nominal stress through the constitutive equations of the material. The stress concentration factor is accounted for through the tensor $\underset{\approx}{\boldsymbol{B}}$. As previously, $\underset{\approx}{\boldsymbol{B}} : \underset{\sim}{\boldsymbol{\Sigma}}$ characterizes the elastic stress field at the critical point. The correction $\underset{\approx}{\boldsymbol{C}} : \underset{\sim}{\boldsymbol{E}}^{p}$ is added to account for the bulk plasticity in the computation of stress and strain fields at the critical point. The method will therefore deliver a greater value for $\underset{\sim}{\boldsymbol{\varepsilon}}^{pI}$ than the linear one which, will result in better estimations in the case of non-confined plasticity and creep loadings as it will be shown in the following.

5.2. Implementation and identification procedure

Basically, the identification procedure consists in a parametric study on different values of the radius R. More precisely, for the AM1 material at high temperature the identification procedure that has been developed includes fatigue and creep results and can be decomposed into three steps:

- Perform elastic-viscoplastic simulations of a creep test and of a fatigue test over a few cycles. This first step is made with the full FE model of the component, like those presented in Fig. 2. The evolution of stresses and strains at the critical point will be used as reference values in the identification procedure.
- Perform an elastic calculation of the specimen and deduce the evolution of $\underset{\sim}{\boldsymbol{\Sigma}}$ under the fatigue loading. For different values of the integration sphere radius R, compute the nominal stresses $\underset{\sim}{\boldsymbol{\Sigma}}_R$. Then, for each radius R, identify the corresponding $\underset{\approx}{\boldsymbol{B}}_R$, $\underset{\approx}{\boldsymbol{C}}_R$ tensors by comparison between the elastic-viscoplastic reference simulations and the estimation using the rule (10).
- Compute the nominal stress tensor $\underset{\sim}{\boldsymbol{\Sigma}}_R$ for creep loading from the elastic FE simulation for each previously defined value of R. The values of $\underset{\sim}{\boldsymbol{\Sigma}}_R$, together with the corresponding $\underset{\approx}{\boldsymbol{B}}_R$, $\underset{\approx}{\boldsymbol{C}}_R$ tensors identified at the previous step, are then used to simulate the response of the correction method using Eq. (10). The final value for the radius R_0, and the corresponding tensors $\underset{\approx}{\boldsymbol{B}}_{R_0}$, $\underset{\approx}{\boldsymbol{C}}_{R_0}$, are the ones giving the better agreement compared to the full FE elasto-viscoplastic creep and fatigue simulations.

Other loading conditions can then be simulated by the correction method, especially those corresponding to the reference solutions, under thousands of successive cycles. The nominal stress $\underset{\sim}{\boldsymbol{\Sigma}}_{R_0}$ for any other loading condition can be directly obtained from the calibration condition, since this quantity is computed from elastic results.

Applications described in the following sections are focused on AM1, that exhibits more viscosity and therefore non-confinement effects.

5.3. Application of the correction method on AM1 $K_t = 1.32$ specimens

The proposed correction method has been applied to the AM1 specimen with $K_t = 1.32$. As for Herbland's method, the $\underset{\approx}{\boldsymbol{B}}$, $\underset{\approx}{\boldsymbol{C}}$ tensors to be identified can be restricted to the following expressions using the Voigt notation:

$$\underset{\approx}{\boldsymbol{B}} = \begin{pmatrix} 0 & 0 & 0 & 0 & 0 & 0 \\ 0 & B_{22} & B_{23} & 0 & 0 & 0 \\ 0 & B_{23} & B_{33} & 0 & 0 & 0 \\ 0 & 0 & 0 & 0 & 0 & 0 \\ 0 & 0 & 0 & 0 & 0 & 0 \\ 0 & 0 & 0 & 0 & 0 & 0 \end{pmatrix} \tag{13}$$

$$\underset{\approx}{\boldsymbol{C}} = \begin{pmatrix} 0 & 0 & 0 & 0 & 0 & 0 \\ 0 & C_{22} & C_{23} & 0 & 0 & 0 \\ 0 & C_{23} & C_{33} & 0 & 0 & 0 \\ 0 & 0 & 0 & 0 & 0 & 0 \\ 0 & 0 & 0 & 0 & 0 & 0 \\ 0 & 0 & 0 & 0 & 0 & 0 \end{pmatrix} \tag{14}$$

Fig. 12 presents the results of the parametric study with the averaging radius ranging from 0.6 to 2.0. The two particular loading conditions used for calibration are: $\sigma_{max}^{nom} = 600$ MPa repeated 5 Hz fatigue and 400 MPa creep. It should be emphasized that the fatigue pictures have been plotted for 16,000 simulated cycles but only the first five cycles have been used in the calibration procedure explained in the previous section.

Whatever the radius value is, the 5 cycles used for the identification are well described. The averaging radius controls the ratcheting effect. The larger R is, the more pronounced ratcheting is. Indeed, when R is small, the macroscopic stress $\underset{\sim}{\boldsymbol{\Sigma}}$ becomes close to the local stress at the notch tip and the correction term $\underset{\approx}{\boldsymbol{C}} : \underset{\sim}{\boldsymbol{E}}^{p}$ does not play a significant role. Errors between the new correction method results and FE simulations have been plotted as a function of the averaging radius in Fig. 13. The discrepancy between the estimated curve y^{MC} and the reference curve y^{EF} is defined by:

$$E = \sqrt{\frac{1}{N}\sum_{i}^{N}\left(y_i^{MC} - y_i^{EF}\right)^2} \tag{15}$$

where N denotes the number of points of the curves. Based on these pictures, the optimal radius value for R is 1.2. The corresponding value for localization tensors are: $B_{22} = 1.33$, $B_{33} = 0$, $B_{23} = 0.2$, $C_{22}/E = 0.74$, $C_{33}/E = 1.04$, $C_{23}/E = 1.23$ where E is the Young modulus. As explained in Section 5.1, $\underset{\approx}{\boldsymbol{B}}$ plays the role of a stress concentration factor. This role is confirmed by the value of B_{22} obtained here, which is very close to the value $K_t = 1.32$ characterizing the specimen. This optimal radius will be used on the same specimen in Section 5.5, with other loading conditions.

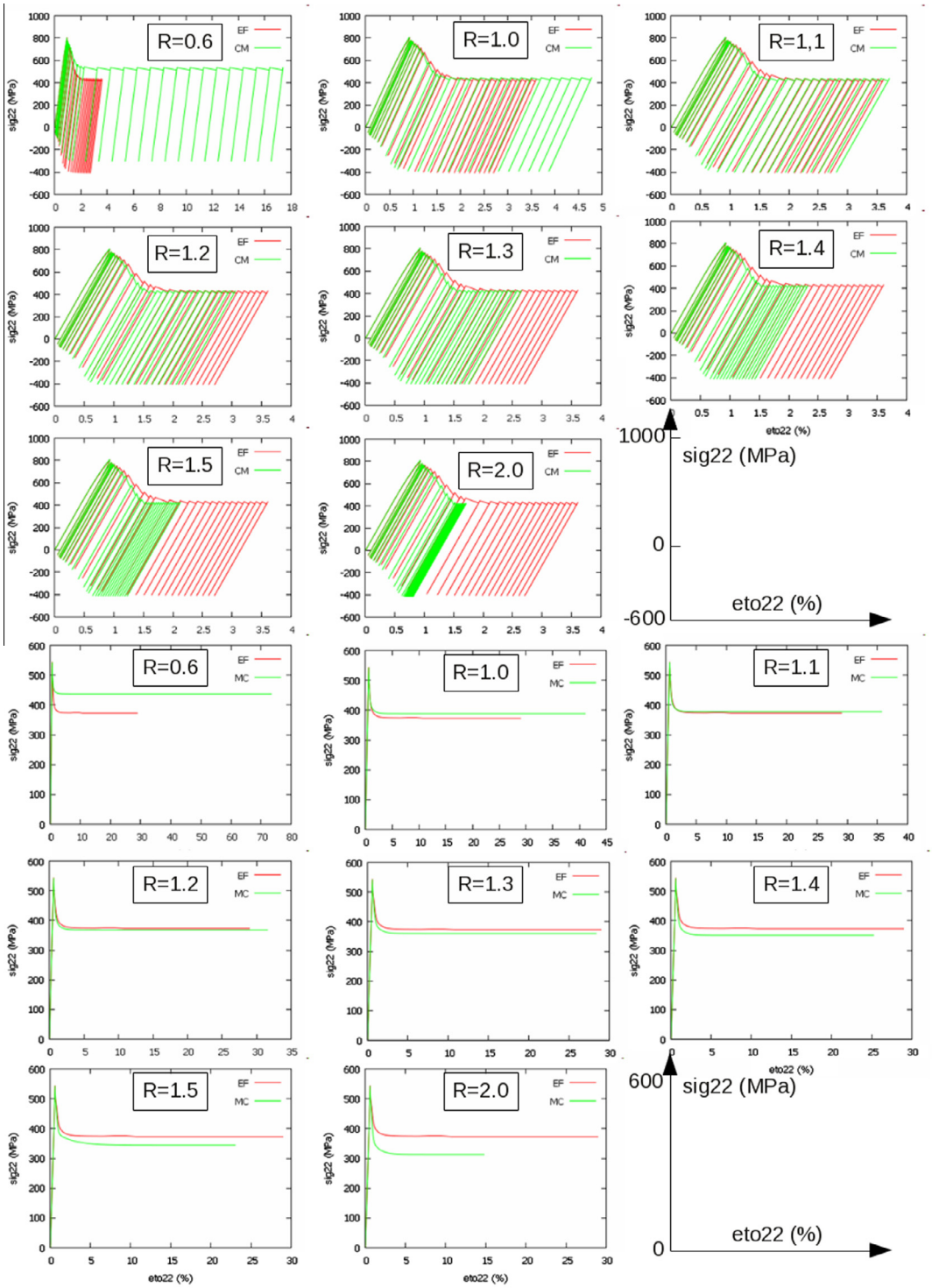

Fig. 12. Parametric study on the averaging radius parameter R of the new correction method for the $K_t = 1.32$ AM1 specimen under 600 MPa repeated fatigue and 400 MPa creep at 950 °C.

5.4. Application of the correction method on AM1 $K_t = 2$ specimens

The same procedure has been applied to the $K_t = 2$ specimen made in AM1 at 950 °C. The calibration loading conditions are:

- 5 Hz repeated fatigue with $\sigma_{max}^{nom} = 600$ MPa;
- 400 MPa creep.

Errors are plotted in Fig. 14 and lead to an optimal averaging radius ranging from 0.5 to 0.6. These values for R are confirmed by comparisons with FE reference simulations presented in Fig. 15. The correction method is better with $R = 0.6$ for the creep condition and with $R = 0.5$ for the fatigue condition. The calibration should be made for $R = 0.55$ to get a better compromise.

5.5. Validation on the $K_t = 1.32$ AM1 specimen

As explained in Section 5.2, the correction method can be directly applied on the same geometry for other loading

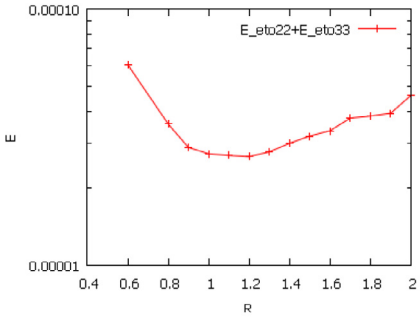

(a) Differences in strains for the 600 MPa fatigue loading

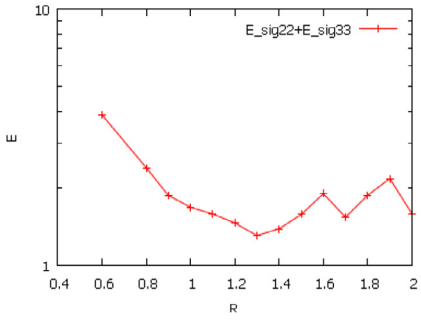

(b) Differences in stresses (in MPa) for the 600 MPa fatigue loading

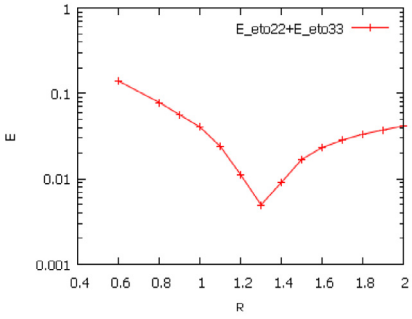

(c) Differences in strains for the 400 MPa creep loading

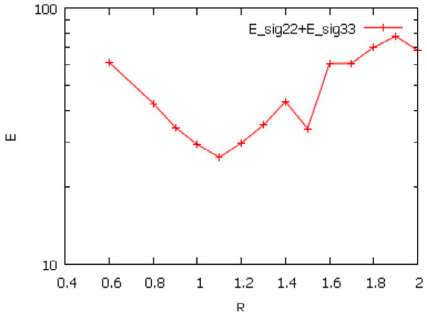

(d) Differences in stresses (in MPa) for the 400MPa creep loading

Fig. 13. Errors between the new correction method results and FE simulation as a function of averaging radius in the identification of the parameters on K_t = 1.32 AM1 specimen.

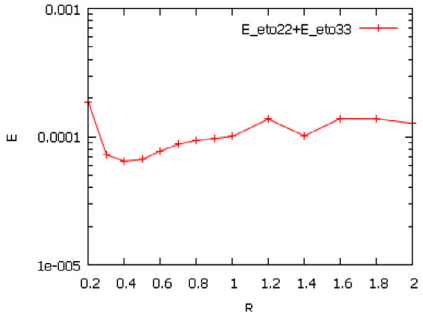

(a) Differences in strains for the 600 MPa fatigue loading

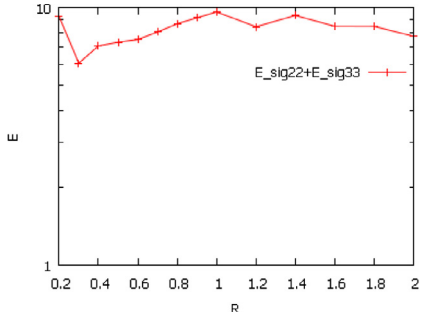

(b) Differences in stresses (in MPa) for the 600 MPa fatigue loading

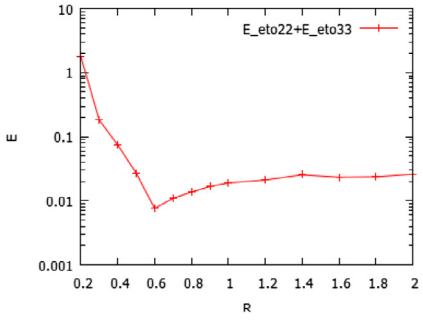

(c) Differences in strains for the 400 MPa creep loading

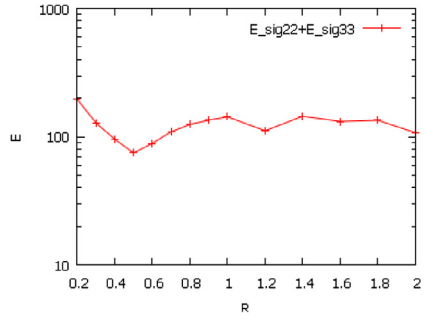

(d) Differences in stresses (in MPa) for the 400 MPa creep loading

Fig. 14. Errors between the new correction method results and FE simulation as a function of averaging radius in the identification of the parameters on K_t = 2 AM1 specimen.

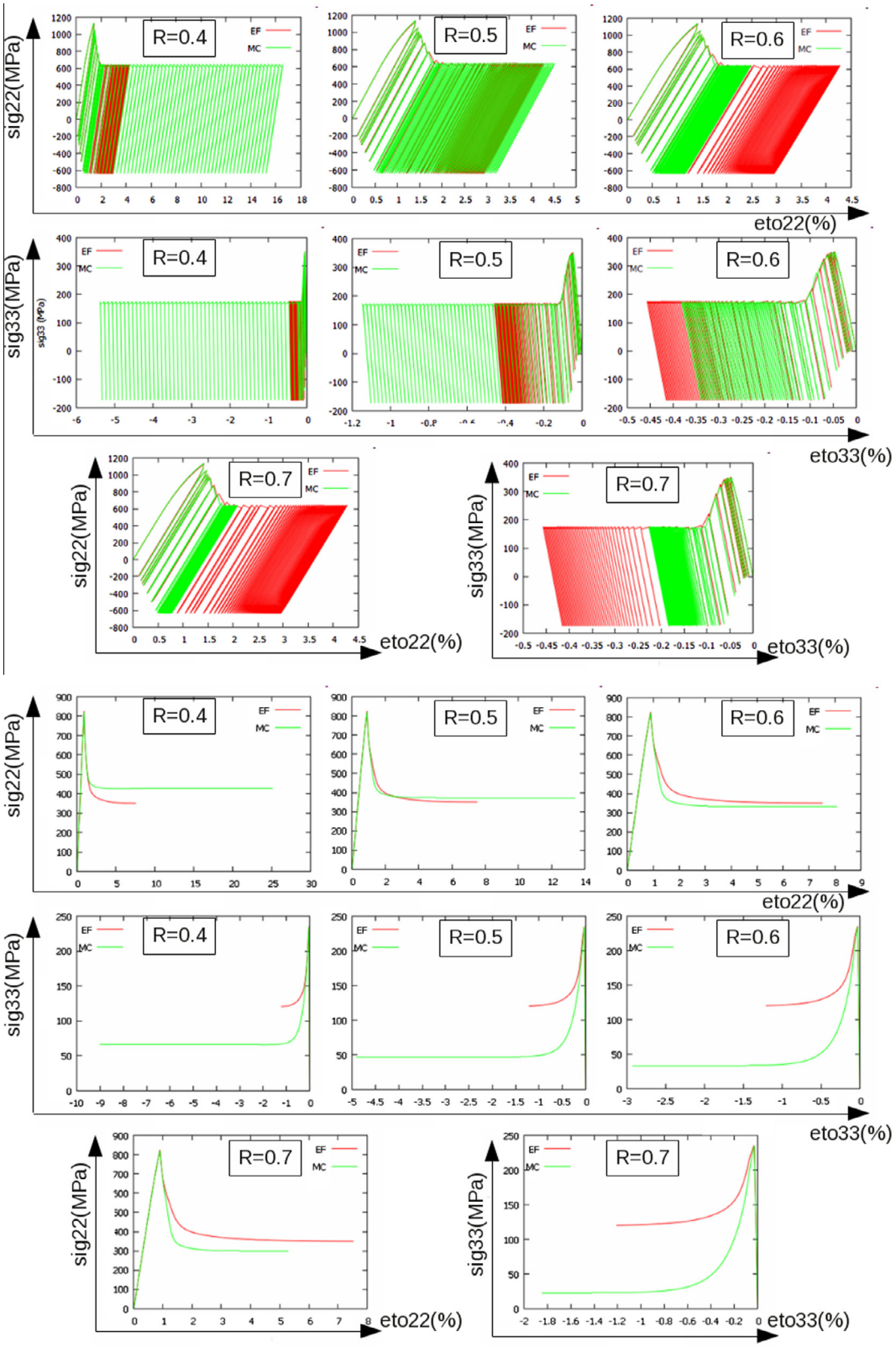

Fig. 15. Parametric study on the R parameter of the new correction method for the $K_t = 2$ AM1 specimen under 600 MPa repeated fatigue (top) and 400 MPa creep at 950 °C (bottom).

conditions. Three cases are presented in Fig. 16, all for the $K_t = 1.32$ geometry:

- 400 MPa 5 Hz repeated fatigue;
- 200 MPa creep;
- 200 MPa fatigue with 90 s holding time.

Correction method simulations are compared to full elastic-viscoplastic FE simulations. A very good agreement is found for all cases.

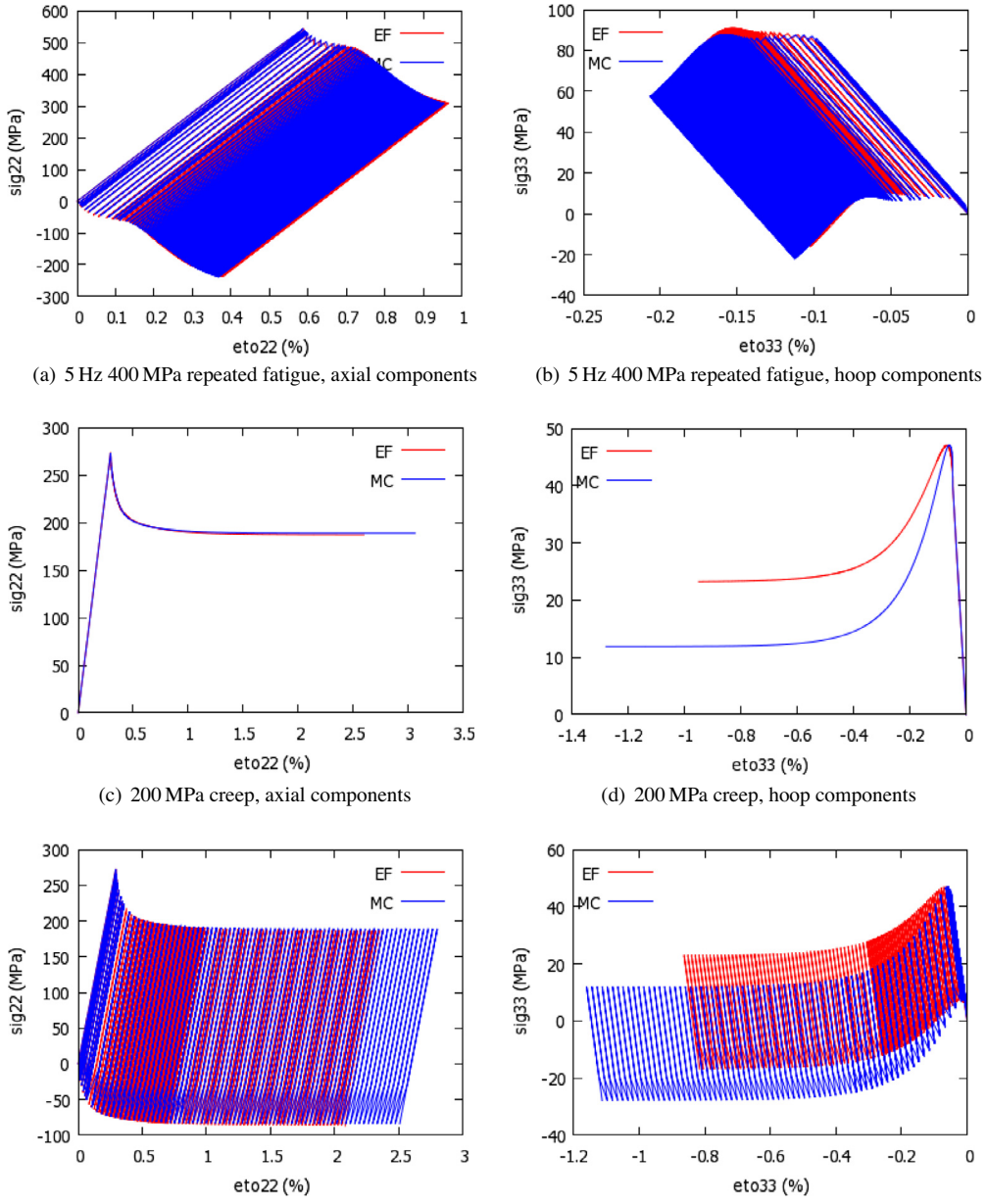

(a) 5 Hz 400 MPa repeated fatigue, axial components

(b) 5 Hz 400 MPa repeated fatigue, hoop components

(c) 200 MPa creep, axial components

(d) 200 MPa creep, hoop components

(e) 200 MPa repeated fatigue with 90s holding time, axial components

(f) 200 MPa repeated fatigue with 90s holding time, hoop components

Fig. 16. Application of the new correction method on K_t = 1.32 AM1 specimen under 400 MPa 5 Hz repeated fatigue, 200 MPa creep and 200 MPa repeated fatigue with 90 s holding time at 950 °C. The new correction method results are plotted in blue whereas the FE elasto-viscoplastic simulations are plotted in red. (For interpretation of the references to color in this figure legend, the reader is referred to the web version of this article.)

6. Application on a multi-perforated tube specimen

Finally, Herbland's methods and the new correction method have been validated and compared on a structural specimen made in AM1. It consists in a tubular multi-perforated piece representative of turbine blades geometries. It is 14 mm in diameter and 1 mm thin. Nine inclined holes whose diameter is 0.5 mm have been perforated with an angle of 60° from the tube axis.

The specimen is submitted to axial loading conditions along the longitudinal direction (x_1 axis) at one end, the other displacement degrees of freedom remaining equal to zero at the other end. Given the geometry and loading conditions, only one half of the specimen has been meshed using linear tetrahedron elements as presented in Fig. 17. Both the inelastic analyses made for the calibration (over one or a few cycles) and the ones for the complete reference solution (thousands of cycles) are performed with the same FE model and the same constitutive equations.

There is an interaction between holes, due to the geometrical configuration, and the small distance between them. Consequently a full elasto-viscoplastic simulation over one cycle must be used to identify the critical point. The chosen critical element is located on the outer surface of the central hole, as seen in Fig. 18.

The difficulty of this case comes from the fact that Gauss Points in the critical element are not exactly located at a free surface, resulting in a complex stress state. This effect is emphasized by the chosen element size, that is coarse to preserve FE analysis tractability. To simplify the calibration procedure of the correction methods, the stress and strain tensor at the critical Gauss Point

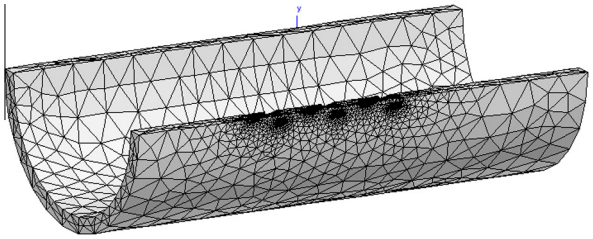

Fig. 17. Mesh of the multi-perforated specimen made in AM1. The longitudinal axis is denoted x_1, x_2 being vertical.

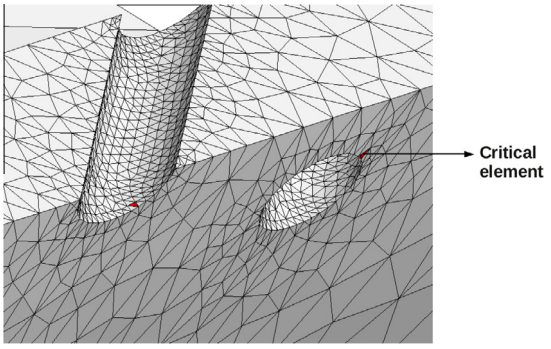

Fig. 18. Critical element chosen for the application of notch correction methods.

have been projected in a plane stress surface element. The corresponding stress tensor writes:

$$\underset{\sim}{\boldsymbol{\sigma}} = \begin{pmatrix} \sigma_{11} & \sigma_{12} \\ \sigma_{12} & \sigma_{22} \end{pmatrix} \tag{16}$$

For the sake of simplicity, the shape of the localization tensor in the linear correction method has been identified from the shape of the stiffness tensor and only 9 components, namely $C_{11}, C_{12}, C_{13}, C_{22}, C_{23}, C_{33}, C_{44}, C_{55}, C_{66}$ have been considered instead of all the 21 components. In the local plane stress element, this tensor can finally be reduced to four components: $C_{11}, C_{22}, C_{12}, C_{33}$.

The linear correction method and the new method have been applied on a repeated fatigue test at 5 Hz under $\sigma^{nom}_{max} = 400$ MPa at 1000 °C. Simulations of creep under 200 MPa have also been used to calibrate the new method. The linear method identification results in the following value of the localization tensor: $C_{11} = 1.22 \times 10^5$ MPa, $C_{22} = 4.68 \times 10^4$ MPa, $C_{33} = 1.53 \times 10^4$ MPa, $C_{12} = 0$. Fig. 19 presents the results obtained with Herbland's linear correction method, compared to the reference calculation made over 8000 cycles. As for the notched specimens, the stresses at stabilization are correctly predicted but the ratcheting effect on deformation is not accounted for.

Regarding the new correction method, we have chosen to neglect the σ_{12} components, so that only three components are left for each tensor (B_{11}, B_{22} and B_{12}). To do so, the principal stress frame is used, unlike what has been done for the linear method. The calibration procedure explained in Section 5.2 has been applied. Errors in strains and stresses for the creep loading are presented in Fig. 20. Together with the fatigue simulation, it leads to an averaging radius $R = 0.3$ mm which is a compromise between fatigue and creep results. Figs. 21 and 22 show the results of the correction method on 8000 simulated cycles and creep loading respectively. The assumption on the 12 component of the stress tensor is validated for both creep and fatigue loadings. Rachetting effect is slightly over-estimated in the case of fatigue, but the stress amplitude and mean values are in good agreement with FE results

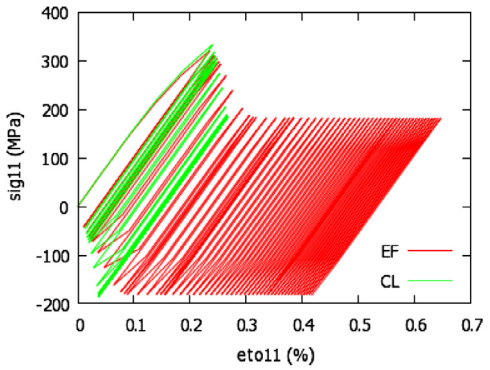

(a) 11 components

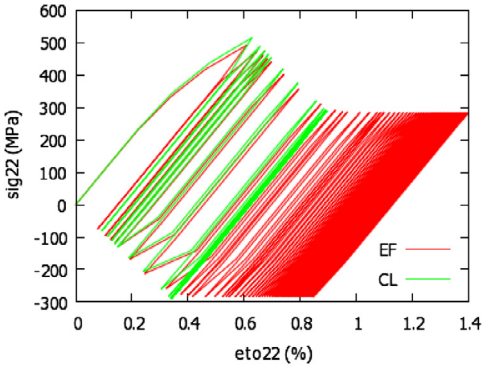

(b) 22 components

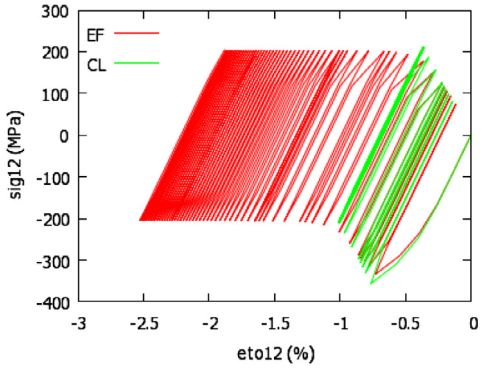

(c) 12 components

Fig. 19. Simulation of 8000 cycles with the linear correction method on the AM1 multi-perforated specimen under 400 MPa fatigue loading and comparison with FE simulation.

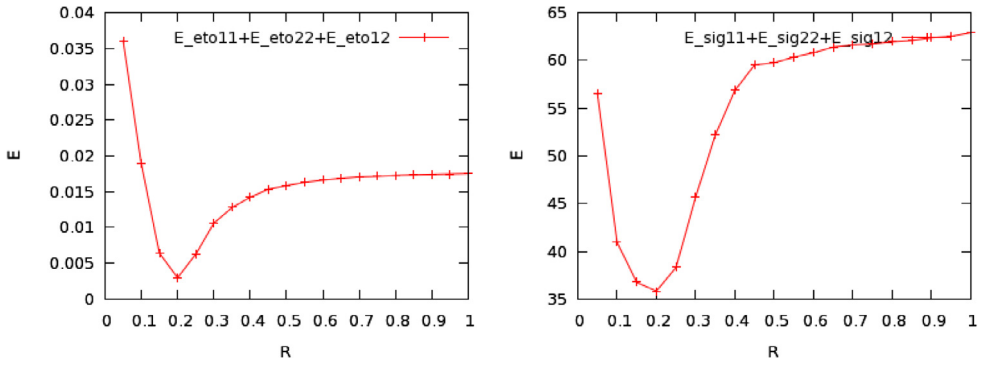

(a) Differences in strains (b) Differences in stresses (in MPa)

Fig. 20. Errors in stresses and strains between the FE simulation and notch correction method identification on the multi-perforated specimen under 200 MPa creep loading at 1000 °C.

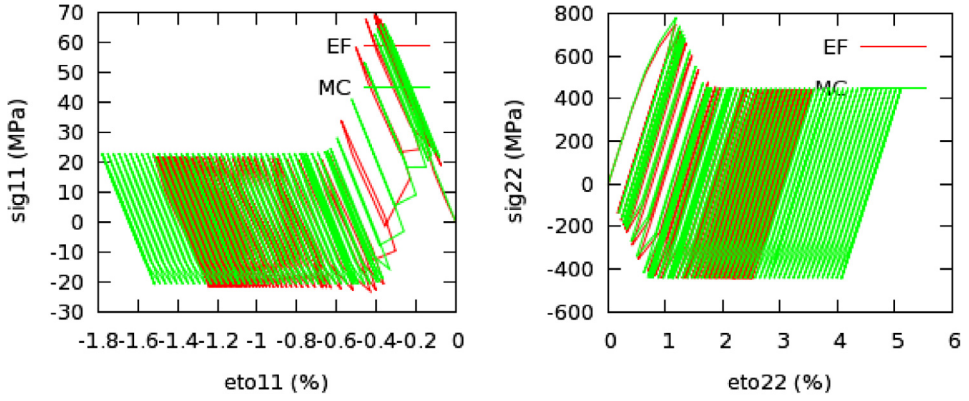

(a) 11 components in the principal stresses frame (b) 22 components in the principal stresses frame

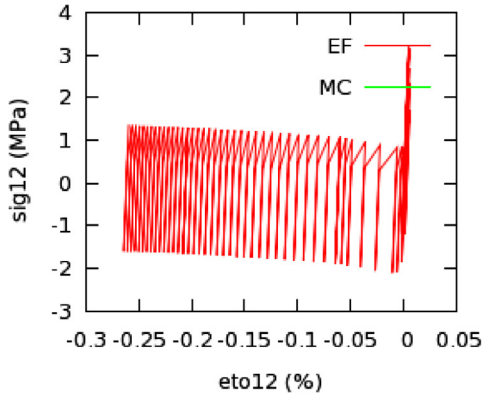

(c) 12 components in the principal stresses frame

Fig. 21. Simulation of 8000 cycles with the new correction method on the AM1 multi-perforated specimen under 400 MPa fatigue loading at 1000 °C and comparison with FE simulation.

at the critical point. Concerning creep, the main component σ_{22} is quite precisely estimated by the method but the σ_{11} component is over-estimated. Both ε_{11} and ε_{22} components are too low compared to the reference elastic-viscoplastic FE simulation.

7. Concluding remarks

The present paper describes innovative methods for a fast estimation of cyclic elastic-viscoplastic stress and strain states at notches based on tools used in the homogenization community. They consist in considering a notch or any other singularity in a structure as an elastic-viscoplastic inclusion in a matrix. Three methods have been successively considered and analyzed:

- Herbland's linear correction method, inspired from Kröner's approach for an inclusion in an elastic matrix;
- Herbland's non-linear correction method which is an extension of the previous one and takes into account plastic accomodation thanks to a β-rule type correction;

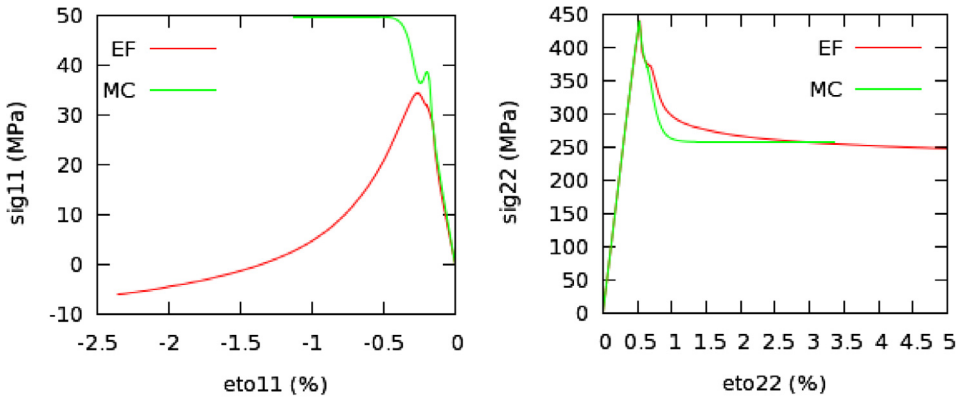

(a) 11 components in the principal stress frame (b) 22 components in the principal stress frame

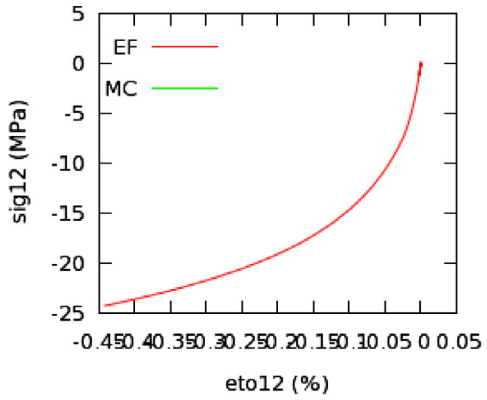

(c) 12 components in the principal stress frame

Fig. 22. Application of the new correction method on the AM1 multi-perforated specimen under a 200 MPa creep loading at 1000 °C and comparison with the reference FE simulation.

- a new correction method which uses the TFA framework. It has been shown to be also an extension of the linear method that account for non-confined plasticity.

The following conclusions can be drawn:

- Herbland's linear correction method should be restricted to confined-plastic zone conditions for which it gives satisfactory results.
- The ratcheting phenomenon can be captured with Herbland's non-linear correction method, provided there is no generalized creep in the structure.
- The new correction method gives good results in all tested cases. It gives precise estimation of stress and strain states at notch for $K_t = 1.32$ and $K_t = 2$ specimens under fatigue and creep. The calibration procedure requires more post treatment simulations since a parametric study is needed to calibrate the averaging radius.
- Correction methods have been validated on a complex multiaxial test case where they give good estimation of stress and strain states at the critical point.

Future works on this topic will focus on the following points:

- There is work still to be done to justify homogenization-type approaches in the notch correction context as emphasized in Herbland et al. (submitted for publication). In particular, the physical meaning of the $\underset{\sim}{\boldsymbol{\sigma}}^M$ quantities in Herbland's methods or $\underset{\sim}{\boldsymbol{\Sigma}}$ in the new one have to be elucidated.
- Links between geometries and materials in one hand and notch correction parameters in the other hand have to be studied. The identification procedures could then be simplified or even suppressed. In the particular case of the new correction method, links between the averaging radius R and the size of the plastic zone should be interpreted. We have also emphasized that $\underset{\approx}{\boldsymbol{B}}$ plays the role of a stress concentration factor and that B_{22} value is very close to the K_t of the considered notch. Finally, spherical averaging volume have been proposed but other shapes could be considered in order to try to increase precision of estimations.
- The methods have to be written in an anisothermal formalism in order to simulate complex loading conditions. The principle that we propose is to normalize C tensor by the Young modulus as a function of temperature $E(T)$. Accordingly, the localization tensors could be taken constant in temperature. This point has to be validated.
- The validation of the new correction method should be followed up, in particular for non-proportional loadings. Herbland have reported good predictions with his methods in that case. There is no reason that the new correction method should fail since it uses a similar formalism.
- Finally, those methods are most of the time used in a lifetime prediction context. Estimations of the impact of correction methods errors on the calculated lifetime compared to full FE simulations should be studied. Obviously, results will depend on the damage law formalism considered. Indeed, if damage evolution is stress dependent, such as in Onera model (Chaboche and Lesne, 1988), the goal of the correction method

should be to estimate precisely the evolution of the stress amplitude and mean stress. However, strain type or mixed damage model formulations will require precise description of ratcheting. Accordingly, we think that the new correction method will be a powerful tool in that context.

Acknowledgments

The authors gratefully acknowledge the French Ministry of Defence and Safran Snecma and Turbomeca companies for the financial support of this study through the project "PRC Durée de Vie des Structures Chaudes".

References

Barkey, M.E., Socie, D.F., Hsai, K.J., 1994. A yield surface approach to the estimation of notch strains for proportional and nonproportional cyclic loading. J. Eng. Mater. Technol. 116, 173–179.

Berveiller, M., Zaoui, A., 1978. An extension of the self-consistent scheme to plastically-flowing polycrystals. J. Mech. Phys. Solids 26, 325–344.

Buczynski, A., Glinka, G., 2003. An analysis of elasto-plastic strains and stresses in notched bodies subjected to cyclic non-proportional loading paths. In: Carpinteri, A., de Freitas, M., Spagnoli, A. (Eds.), Sixth International Conference on Biaxial/Multiaxial Fatigue and Fracture, European Structural Integrity Society, vol. 31. Elsevier, pp. 265–283.

Cailletaud, G., 1987. Une approche micromécanique phénoménologique du comportement inélastique des métaux (Ph.D. thesis). Université de Paris VI.

Chaboche, J.L., 2008. A review of some plasticity and viscoplasticity constitutive theories. Int. J. Plast. 24 (10), 1642–1693.

Chaboche, J.L., Lesne, P.M., 1988. A non-linear continuous fatigue damage model. Fatigue Fract. Eng. Mat. Struct. 11 (1), 1–17.

Chaboche, J.L., Kanouté, P., Azzouz, F., 2012. Cyclic inelastic constitutive equations and their impact on the fatigue life predictions. Int. J. Plast. 35, 44–66.

Chaudonneret, M., Culié, J.P., 1985. Adaptation of Neuber's theory to stress concentration in viscoplasticity. La Rech. Aérosp. 4, 33–40.

Desmorat, R., 2002. Fast estimation of localized plasticity and damage by energetic methods. Int. J. Solids Struct. 39, 3289–3310.

Dvorak, G., Benveniste, Y., 1992. On transformation strains and uniform fields in multiphase elastic media. Proc. R. Soc. Lond. 437, 291–310.

Guo, W., Wang, C.H., Rose, L.R.F., 1998. Elastoplastic analysis of notch-tip fields in strain hardening materials. Tech. Rep. DSTO-RR-0137, Aeronautical and Maritime Research Laboratory.

Herbland, T., Cailletaud, G., Quilici, S., submitted for publication. An adaptative technique for a fast estimation of local stress and strain states at notch root under multiaxial random loadings. Int. J. Fatigue.

Hoffman, M., Seeger, T., 1985. A generalized method for estimating elastic–plastic notch stresses and strains. Part I: Theory. J. Eng. Mater. Technol. 107, 250–254.

Köttgen, V.B., Barkey, M.E., Socie, D.F., 1995. Pseudo stress and pseudo strain based approach to the notch strain based approaches to multiaxial notch analysis. Fatigue Fract. Eng. Mater. Struct. 18, 981–1006.

Moftakhar, A., 1994. Calculation of Time-Independent and Time-Dependent Strains and Stresses at Notches (Ph.D. thesis). The University of Waterloo, Ontario.

Molski, K., Glinka, G., 1981. A method of elastic–plastic stress and strain calculation at notch root. Mater. Sci. Eng. 50, 93–100.

Neuber, H., 1961. Theory of stress concentration for shear-strained prismatic bodies with arbitrary non-linear stress–strain law. J. Appl. Mech. 28, 544–551.

Ye, D., Matsuoka, S., Suzuki, N., Maeda, Y., 2004. Further investigation of the Neuber's rule and the equivalent strain energy density (ESED) method. Int. J. Fatigue 26, 447–455.

Z-set, Material and structure analysis suite. URL:<http://www.zset-software.com>.